Enhancement of an Optical Fiber Sensor: Source Separation Based on Brillouin Spectrum

Edouard Buchoud, Valeriu Vrabie, Jerome I. Mars, Guy d'Urso, Alexandre Girard, Sylvain Blairon, Jean-Marie Henault

Enhancement of an Optical Fiber Sensor: Source Separation Based on Brillouin Spectrum

E. Buchoud[*1], V. Vrabie[2], J.I. Mars[1], G. D'Urso[3], A. Girard[3], S. Blairon[3], and J-M. Henault[3]

[1]GIPSA-Lab, Department Image and Signal Processing, Grenoble Institue of Technology, BP 46, 38402 Saint Martin d'Hères, France

[2]Centre de Recherche en STIC (CReSTIC), Université de Reims, BP 1039, 51687 Reims, France

[3]Direction R&D, Electricité de France (EDF), 6 quai Watier, 78401 Chatou, France

Tel: +33 (0)4 76 82 71 07 Fax: +33 (0)4 76 57 47 90

E-mail: edouard.buchoud@gipsa-lab.grenoble-inp.fr

***Abstract*—Distributed optical fiber sensors (DOFS) have gained an increasingly prominent role in structural-health monitoring. These are composed of an optical fiber cable in which a light impulse is launched by an opto-electronic device. The scattered light is of interest in the spectral domain: the spontaneous Brillouin spectrum is centered on the Brillouin frequency, which is related to the local strain and temperature changes in the optical fiber. When coupled to an industrial Brillouin optical time-domain analyzer (B-OTDA), an optical fiber cable can provide distributed measurements of strain and/or temperature, with a spatial resolution over kilometers of 40 cm. This article focuses on the functioning of B-OTDA device, where we address the problem of the improvement of spatial resolution. We model a Brillouin spectrum measured within an integration base of 1 m as the superposition of the elementary spectra contained in the base. Then, the spectral distortion phenomenon can be mathematically explained: if the strain is not constant within the integration base, the Brillouin spectrum is composed of several elementary spectra that are centered on different local Brillouin frequencies. We propose a source separation methodology approach to decompose a measured Brillouin spectrum into its spectral components. The local Brillouin frequencies and amplitudes are related to a portion of the integration base where the strain is constant. A layout algorithm allows the estimation of a strain profile with new spatial resolution chosen by the user. Numerical tests enable the finding of the optimal parameters, which provides a reduction to 1 cm of the 40-cm spatial resolution of the B-OTDA device. These parameters are highlighted during a comparison with a reference strain profile acquired by a 5-cm-resolution Rayleigh scatter analyzer under controlled conditions. In comparison to the B-OTDA strain profile, our estimated strain profile has better accuracy, with centimeter spatial resolution.**

***Index Terms*— Brillouin optical time domain analyzer, non-negative least-squares algorithm, non-negative matrix factorization, Rayleigh scattering measurements, structural-health monitoring**

I. Introduction

The durability of civil infrastructures is a crucial issue that can have major economical, social and environmental impact. In civil engineering, many aging infrastructures can become vulnerable in terms of their stability, due to internal erosion, climatic conditions, and other natural phenomena. Infrastructure owners and users can face difficult challenges, such as the optimization of maintenance and the extension of the service life.

Structural-health monitoring is considered a key procedure in industrial processes, because it provides a real-time diagnosis of the state of wear/ damage of a structure. In this context, the major owner of dykes and dams in France, the Electricité de France (EDF) company, is in charge of the monitoring of these industrial structures. Conventional methods to check the stability of dykes are usually based on visual inspections on sites. The measurement of different parameters is also used to provide indicators, such as pressure, flow, temperature, and strain. The systems currently used are based on measurements of self-potential, resistivity and temperature [1]-[4]**.** While the self-potential and the resistivity methods provide efficient measurements, the drawback is that these methods are still manual and require careful placement and use of electronic equipment at the site.

Complementary to these sensors, distributed optical fiber sensors (DOFS) have new issues as passive and semi-automatic solutions. DOFS use low-cost telecommunication grade optical fiber, and a large number of sensors can be multiplexed to enhance their economic viability. Due to their robustness, immunity to electromagnetic interference, and deployment in harsh environments [5], DOFS are attractive tools for structural-health monitoring, to perform distributed strain and temperature measurements. This kind of sensor has found applications in civil-structure monitoring [6], geotechnical engineering [7]-[8], and the aerospace industry

[9]. DOFS offer a multitude of advantages, such as reduced weight and dimensions, strong immunity to electromagnetic interference, environmental robustness, long-gauge measurements, and low cost [10]. For these reasons, in addition to traditional sensors, EDF uses DOFS to monitor dykes and dams, and to detect and locate water leakage [11] and internal erosion [12].

DOFS are composed of an opto-electronic device that is linked to an optical fiber cable, which provides the sensing element. The opto-electronic device, which is classically known as the interrogator, launches a light impulse into the optical fiber and records the backscattered light. Three phenomena are identified: the Raman, Brillouin, and Rayleigh scatterings. The Raman scattering is only dependent on the temperature in the optical fiber cable, while the Brillouin and Rayleigh scatterings can be linked to the temperature and strain changes. Several devices take advantage of these phenomena to measure the distribution of temperature and strain profiles along fiber optics. The Rayleigh device has the advantage that it can be used to provide centimeter spatial resolution, although in this configuration the sensor length is limited to 70 m [13]. Whereas the Brillouin devices provides measurements over kilometers, although a meter spatial resolution [14]. However, to monitor important structures, the needs of EDF indicate centimeter spatial resolution with a sensing length of over 5 km. We need to understand and model the Brillouin spectra recorded by these devices to enhance the spatial resolution while maintaining the same sensing length.

For over two decades, DOFS based on Brillouin scattering devices have gained significant interest as they can be used to monitor temperature and strain in large infrastructures, thus replacing thousands of classical sensors. The thermal and strain sound-wave agitations in the optical fiber cable result in acoustic waves that induce refractive index fluctuations in the optical fiber. This phenomenon means that the incident light waves are scattered with shifted frequencies. Various industrialized devices are based on Brillouin scattering. They exploit the interaction of light with the acoustic phonons that propagate in the fiber core. This interaction induces a spontaneous Brillouin spectrum that is centered on a Brillouin frequency that is related to the local temperature and strain conditions in the optical fiber [14]. Classical Brillouin optical time-domain analyzers (B-OTDAs) are based on this stimulation of Brillouin scattering. The industrial B-OTDA devices have the advantage of a gauge length of 25 km, although the spatial resolution of 40 cm [15] is not enough for many applications.

In recent years, increasing attention has been paid to the improvement of the spatial resolution, while maintaining the same measurement performance and gauge length. Many promising studies have been carried out in optical physics [15] to fulfill this goal; e.g., pre-pumping of the acoustic waves can achieve a spatial resolution in the centimeter range [15]. These methods are still under laboratory development. Other studies have been based on the observation of the Brillouin spectra. Ravet *et al.* (2006) highlighted the Brillouin distortion phenomena [16]: when a local and substantial load is applied within the spatial resolution, the measured Brillouin spectrum becomes distorted from an asymmetric form to multiple peaks. They proposed a deconvolution technique to detect and quantify centimeter-long defects applied to the optical fiber cable [17]. This technique relies on an optical physics model, whose parameters include strain distribution within the base integration, extension rate, intensity and frequency of the light waves, and sensing length [17]. The main drawback in our case is that these parameters are not provided by industrial B-OTDA units. The Ravet method is not suitable in our case.

Our previous studies have strengthened the observation and quantification of the Brillouin distortion phenomena within industrial devices under semi-controlled conditions [18]. In this report, we propose another model that is based on signal-processing techniques. The shape of the spontaneous Brillouin spectrum is changed by the acquisition system [19], from a Lorentzian to a Gaussian distribution. This can be modeled using a transfer function that depends on the acquisition system, and thus the optical physics parameters are not needed anymore. Then, we assume that the Brillouin spectrum measured within the B-OTDA device integration base is the sum of several Brillouin spectra that are centered on local Brillouin frequencies. Therefore, if the strain is not constant within the integration base, then the resulting spectrum will be distorted, as has been observed previously. Going beyond this particular study, we emphasis here that the analysis of a distorted spectrum by a source separation technique allows the estimation of its spectral components. Their central frequencies and amplitudes are linked to a constant strained portion within the integration base. Due to this property, a layout methodology within the integration base is needed to provide centimeter resolution measurements. Keeping the same DOFS with an industrial B-OTDA device allows centimeter strain measurements to be achieved.

Numerical and experimental tests with a B-OTDA device were here carried out under laboratory conditions. A Rayleigh device that provides 1-cm spatial resolution measurements over the same optical fiber cable is considered as the reference in this study [20]. This reference serves for comparison purposes with the output of our method. We show that our methodology enables centimeter resolution strain measurements with an industrial B-OTDA unit. In addition, the accuracy of the DOFS is enhanced where the strain variations are important within the spatial resolution. This kind of process is entirely new in the application domain.

We start in section II with a description of the principle of the acquisition using a B-OTDA device. We focus on the interpretation of the Brillouin spectra and propose a model to define its functioning. The theoretical formulation of the problem is presented in section III, using the advanced technique of non-negative source factorization. After a brief theoretical description of the non-negative least-squares (NNLS) algorithm, a scheme is proposed to retrieve the Brillouin frequency profile that allows the reconstruction of the strain profile along the optical fiber cable. Section IV presents two applications of the proposed methodology. The first is a numerical dataset, with a comprehensive discussion about the parameters involved in the algorithm, which provides an understanding of their influence on the new sampling and the results. The second application includes an experimental dataset, with a comparison between the reference Rayleigh measurement and the output of the proposed method,

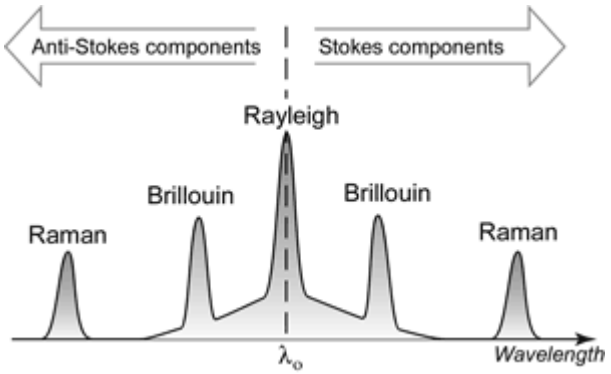

Fig. 1. Illustration of the backscattering spectrum of a monochromatic wave in an optical fiber. Three scattering phenomena appear: the Rayleigh, Brillouin, and Raman scatterings. Their frequencies depend on the strain and/or temperature in the silica of the optical fiber [5].

which provides validation of our methodology. The conclusions follow in section V, which arise from the results of the previous sections, and which emphasize the further applications to which this methodology can be applied.

II. Acquisition Principle and Data Interpretation

A. Distributed Sensing For Temperature and Strain Monitoring

DOFS are composed of an optical fiber cable that is linked to an opto-electronic device. The sensing cable is composed of several optical fibers that are made of silica and are wrapped in a protective coating. The opto-electronic device, which is classically known as the interrogator, launches a light impulse at wavelength λ_0 into the optical fiber and records the backscattered light.

In the frequency domain, three distinct phenomena can be highlighted in the backscattered light, as illustrated in Fig. 1. The first is Rayleigh scattering, which is due to fluctuations in the silica density and composition. The light returns with the same frequency, but parts of the power have been frequency spread, which is called the Rayleigh wing. The second phenomenon is Brillouin scattering, which is due to photon-phonon interactions. This is characterized by a shifted frequency spectrum in the Stokes and anti-Stokes components. These two phenomena are both sensitive to temperature and strain changes in the optical fiber cable, and they are fully explained below. The third phenomenon, the Raman effect, is caused by thermal molecular vibrations, although this is not considered further here. The Raman effect is only temperature sensitive.

Monitoring structures using this kind of sensor consist of installing a sensing cable into the structure, as illustrated in Fig. 2 (top panels). The opto-electronic device provides temperature or strain measurements, depending on the distance into the optical fiber cable. Previous studies in collaboration with EDF have enabled the detection of water leakage in industrial dams using the Raman effect [11]. A Rayleigh-based optical backscatter reflectometer unit (OBR) provides 1-cm spatial resolution, although its drawback is the limited sensing length [13]. In the present report, measurements provided by the Rayleigh OBR will be considered as the reference measurements, due to their high spatial resolution and precision.

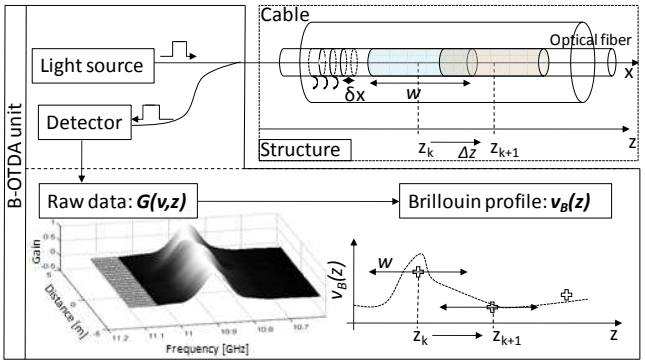

Fig. 2. Ilustration of the B-OTDA-based DOFS. The opto-electronic unit (the industrial B-OTDA) is coupled to the optical fiber cable. The B-OTDA device records a Brillouin spectrum matrix that depends on the distance and frequency. The B-OTDA device has a data-processing unit that estimates the Brillouin profile at each position z_k as the abscissa of the maximum of the measured Brillouin spectrum within the integration base *w*.

However, the goal of EDF is the monitoring of long structures, such as dams. Therefore, their need is for a distributed strain sensor with a sensing length of over 5 km. These qualities can be fulfilled by Brillouin technology. Several devices based on the Brillouin phenomenon exist, but the present report focuses on the industrial B-OTDA device. The goal of this section is to understand its functioning and to model the recorded Brillouin spectra.

The OTDR technique consists of injection of monochromatic light into the optical fiber and measurement of the backscattered intensity, which depends on time. Depending on the optical index n_g in the sensing medium and the period of the pulse round-trip Δt, the localization z of the pulse is given by:

$$z = \frac{\Delta t}{2n_g} c \tag{1}$$

where c is the light velocity in the medium. The smallest distance Δz between two independent measurements is defined as the spatial resolution. Based on this principle, the use of Brillouin scattering in optical fiber sensing was first proposed in 1989 by Horiguchi and Tateda [22]. They showed that local temperature and strain variations in the optical fiber induce local changes in the density and tension of the silica. The consequence is the appearance of a local velocity of the acoustic phonons, called acoustic waves. Interaction of phonons with photons will shift the photon frequency proportionally. Thus, the Brillouin scattered light will be frequency shifted depending on the temperature and strain changes. The Brillouin frequency v_B is given by following formula [14]:

$$v_B(x) = \frac{2n_{eff}(x)V_a}{\lambda_0} \tag{2}$$

where n_{eff} is the effective mode refractive index of the fiber as a function of the curvilinear abscissa *x*, V_a is the velocity of sound in glass, and λ_0 is the wavelength of the monochromatic light. Measurements of this frequency shift are in the range of 9 GHz to 13 GHz for a wavelength of around 1.3 µm to 1.6 µm in standard single mode communication fibers.

Based on the stimulated Brillouin scattering, B-OTDA devices use a pump-probe wave approach. This involves launching a short pump pulse at a frequency v_p into one extremity of the test fiber, and a continuous wave (CW) probe beam at a frequency v_{CW} into the other end. The width of the light impulse is noted as τ and an energy transfer occurs between the two waves when they encounter each other in the optical fiber. When the frequency difference $v = |v_{CW} - v_p|$ is equal to the Brillouin frequency in the optical fiber, the energy transfer is maximum. Then, the CW probe intensity will vary along the fiber depending on time and frequency. By measuring the time-dependent CW signal over a wide range of frequency differences *v*, it is possible to localize the position through Eq. (1). The width of the impulse is linked with the scanned portion of the optical fiber, known as the integration base, *w*, whereby:

$$w = v_g \frac{\tau}{2} \tag{3}$$

where v_g is the pulse group velocity in the optical fiber. As an example, a 10-ns pulse width provides a meter integration base. The integration base is centered on *z*, which is the sensing acquisition point. Spatial redundancy appears between two adjacent acquisition points when the spatial resolution Δz is less than *w*. Fig. 2 (bottom panel) illustrates how the link between these parameters is defined. Thus, for each position *z* of the optical fiber, a stimulated Brillouin spectrum is measured. These spectra are centered on $\boldsymbol{v_B(z)}$, but their shape varies between Lorentzian and Gaussian distributions depending on the acquisition parameters, such as: the intensity and frequency of the pump and probe waves, and the extension rate, τ. [23]. A classical effect is that the spectrum broadens when the width of the pump pulse becomes shorter than 10 ns.

B. Data Interpretation and Mathematical Modeling

The state of the art in data interpretation and modeling of the B-OTDA unit tells us that this type of sensor has been widely studied. Bao *et al.* [14] proposed a theoretical model to describe the behavior of a DOFS. Based on coupled wave equations and optical physics, the CW beam can be modeled according to distance. Ravet *et al.* [17] modeled a Brillouin spectrum that depended on the strain distribution within the integration base, *w*. Several types of parameters were considered in their models: the power of the two beams, the extinction rate of the beam, the length of the sensor, the integration base and finally the spatial sampling. The first three of these are linked to the optical part of the device and cannot be chosen by the user; these are not provided in our case. The last two are chosen by the user and are well defined. Therefore, these processes cannot be applied to an industrial device like the DITEST STA-R. To our knowledge, no other studies have modeled the Brillouin spectra recorded by B-OTDA devices without the use of optical parameters.

This part of the present article is dedicated to the understanding of the phenomena linked to the device functioning as a signal processor. Taking into account that the spontaneous Brillouin spectrum $\boldsymbol{S_N(v)}$ shape is spoiled by the device, as was shown by Ravet *et al.* [17], we have defined a transfer function $\boldsymbol{F(v)}$. This transfer function depends on the acquisition parameters, although its dependency is not considered here. The convolution product between $\boldsymbol{S_N(v)}$ and $\boldsymbol{F(v)}$ gives an elementary Brillouin spectrum, $\boldsymbol{S_e(v)}$, which is expressed as:

$$S_e(v) = S_N(v) * F(v) \tag{4}$$

The shape of the elementary spectrum will evolve between Lorentzian and Gaussian distributions, depending on the acquisition parameters.

Considering an infinitesimal part *dx* of the optical fiber centered at *x*, the spontaneous Brillouin spectrum is centered on the local Brillouin frequency $v_B(x)$. Due to the convolution, $S_e(v)$ is also centered on $v_B(x)$. As the device has an integration base of *w*, the Brillouin spectrum $\widetilde{\boldsymbol{G}}(\boldsymbol{v}, \boldsymbol{z_k})$ measured by the B-OTDA unit at the acquisition point z_k along the fiber optic cable is modeled here as the integration of all of the local elementary Brillouin spectra contained within *w*:

$$\tilde{G}(v, z_k) = \int_{z_k - w/2}^{z_k + w/2} S_e(v - v_B(x))dx \tag{5}$$

Thus, if the shape of the elementary spectrum can be estimated, deconvolution processing allows the evaluation of the frequencies $v_B(x)$ within *w* for an acquisition point.

C. Brillouin Distortion Phenomenon

In structural-health monitoring, the sensing cable is affected by various factors, such as the ground response of the environmental effects, anomalies (e.g., cracks), and others. In terms of the strain, these anomalies are highly energetic and can be smaller than *w*: a high strain variation within a few centimeters. The goal is to detect and localize these anomalies, to optimize the maintenance of such structures.

If the strain is not constant within *w*, the Brillouin spectrum becomes distorted. As a consequence, the intensity of the received CW beam will vary depending on the frequency *v*. When *v* is equal to one of the Brillouin frequencies, the intensity will increase in the Brillouin gain spectrum. So the Brillouin spectrum contains multiple peaks for non-constant strain within *w*, whereas the spectrum is a single peak if the strain is constant. This phenomenon has been seen and quantified with experimental data acquired under controlled conditions [16]-[18]. This also highlights the limits of the industrial device: the algorithm of the industrial B-OTDA device does not take into account the Brillouin distortion.

We propose a description of this phenomenon founded on the proposed model (see Eq. (5)). As the Brillouin spectrum is the sum of the local spectra within *w*, when the strain is not constant (see Fig. 3a), the centers of these spectra vary depending on *x*. The Brillouin spectrum that is measured by the industrial B-OTDA device is distorted, as shown in Fig. 3b. Based on Eq. (5), it is possible to link the distortion of the spectrum with the shape of the local Brillouin frequencies. Dividing the integration base *w* into segments of size δx in which we assume that the strain is constant, we can rewrite Eq. (5) as:

$$\tilde{G}(v, z_k) = \sum_{i=1}^{N-1} \left(\int_{z_k - \frac{w}{2} + i\delta x}^{z_k - \frac{w}{2} + (i+1)\delta x} S_e\big(v - v_B(x)\big)dx \right) \tag{6}$$

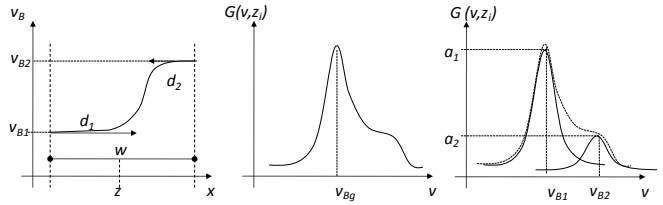

(a) (b) (c)

Fig. 3. (a) Brillouin frequency profile within *w*. (b) The resulting Brillouin spectra. (c) Identification of two elementary Brillouin spectra.

where N is the number of segments, $N = w/\delta x$. N can also be seen as the sum of the spectral components within w. As the strain is assumed to be constant within δx, $\boldsymbol{v_B(x)}$ is constant with δx. This means that the integral of $\boldsymbol{S_e(v\text{-}v_B(x))}$ within $i\delta x$ is equal to $\delta x.\boldsymbol{S_e(v\text{-}v_{Bi})}$. However, as several portions of w might be related to the same value of the strain, they have the same v_{Bi}. Therefore, we assume that the spectrum is a combination of elementary Brillouin spectra that are centered on several local frequencies, v_{Bj}:

$$\tilde{G}(v, z_k) = \delta x. \sum_{j=1}^{P} a_j . S_e\left(v - v_{Bj}\right) \tag{7}$$

where the new indices $j = \{1, .., P\}$ are a subset of $i = \{1, .., N\}$, $\boldsymbol{S_e(v\text{-}v_{Bj})}$ are the spectral components that are contained in the distorted Brillouin, and P is their number. Fig. 3c shows that the distorted spectra of Fig. 3b can be roughly approximated by only two elementary Brillouin spectra. The number of spectral components P that allows the modeling of a measured Brillouin spectrum is an important parameter, and this will be discussed further later. The relative amplitude of the j[th] spectral component can be expressed as a section of w:

$$\widetilde{d_M} = \frac{a_M}{\sum_{j=1}^{P} a_j} . w \tag{8}$$

That is, $\widetilde{d_M}$ is a percentage of the integration base where the portions are similarly stressed.

The identification of the spectral components of a measured Brillouin spectrum leads to the finding of the local frequencies and the related weight of the elementary Brillouin spectra, as shown in Fig. 3c. The next goal is to find the amplitudes and frequencies of the spectral components contained in the distorted spectrum.

D. From Raw Data to Strain Measurement

The raw data recorded by a B-OTDA device is a Brillouin spectrum matrix. This is denoted as $\boldsymbol{G}$, and it depends on the frequency v and the abscissa z_k:

$$\boldsymbol{G} = \left\{ G(v, z_k) \in \mathbb{R}_+ \middle| 1 \le v \le N_v, 1 \le z_k \le N_L \right\} \tag{9}$$

where N_v and N_L are the total acquisition frequency and the number of acquisition points, respectively. The parameters chosen by the user are the integration base w, the spatial resolution Δz, which is given by the length of the optical fiber cable divided by the number of acquisition points, and the frequency sampling Δv. For example, typical values for industrial B-OTDA-based DOFS of 5-km gauge length are a 1-m integration base and a spatial resolution of 40 cm, with the finest frequency sampling available being 1 MHz. Usually, the central frequency v_B of the spectrum is found by optimizing the parameters of a pseudo-Voigt distribution [19]: a Brillouin profile $\boldsymbol{v_B(z)}$ is provided by the B-OTDA device that depends on the distance z, as shown in Fig. 2. Therefore, the accuracy of the frequency profile is dependent on the frequency sampling.

Between two states of the optical fiber cable (reference and stressed), two measurements of $\boldsymbol{v_B(z)}$ are acquired by the device. From these, a relative frequency shift denoted as $\boldsymbol{\Delta v_B(z)}$ is calculated. This is assumed to be proportional to the temperature variations $\boldsymbol{\Delta T(z)}$ and the strain $\boldsymbol{\varepsilon(z)}$ [14] [21], such that:

$$\Delta v_B(z) = C_\varepsilon \varepsilon(z) + C_T \Delta T(z) \tag{10}$$

with C_T and C_ε as the characteristics of the fiber type (which depend on the operating wavelength and the device). For a B-OTDA unit and standard fiber cables operating at λ_0 = 1550 nm, typical values of these coefficients are 1 MHz/°C and 0.05 MHz/με, respectively [13].

III. Non-Negative Source Separation Methodology

A. Data Decomposition

Our issue is similar to a deconvolution problem. Several algorithms can be fit to solve it, such as inverse problem frameworks and Bayesian approaches, among others. Our spectra are positive, and the shape of the elementary Brillouin spectrum can be estimated for an optical fiber cable, where a straightforward solution is to use the non-negative matrix factorization formulation.

1) Non-Negative Matrix Factorization

Given a Brillouin matrix, we have to define the elementary Brillouin spectra that are contained within each Brillouin spectrum recorded. Thus, the problem can be formulated as:

$$\boldsymbol{G} \cong \boldsymbol{SA} \tag{11.a}$$

$$\boldsymbol{C} = \|\boldsymbol{G} - \boldsymbol{SA}\|_2^2 \tag{11.b}$$

where $\boldsymbol{G} \in \mathbb{R}_+^{N_v \times N_L}$ represents the Brillouin matrix (the Brillouin spectra recorded by the B-OTDA device at the acquisition points are the columns of $\boldsymbol{G}$), $\boldsymbol{S} \in \mathbb{R}_+^{N_v \times N}$ designates the source matrices, and $\boldsymbol{A} \in \mathbb{R}_+^{N \times N_L}$ represents the weight associated to each source. N is the number of possible spectral components.

The problem is thus to define matrices $\boldsymbol{S}$ and $\boldsymbol{A}$ from the observation matrix $\boldsymbol{G}$ while minimizing the quadratic error $\boldsymbol{C}$ between the observation data and the estimation, with the only hypothesis being that the shape of the sources is known as the elementary Brillouin spectrum, $\boldsymbol{S_e(v)}$.

2) Source Dictionary Definition

Taking into account Eq. (6), a Brillouin spectrum is a combination of the spectral components with the shape of $\boldsymbol{S_e(v)}$ that are centered in several local frequencies. Therefore,

the elementary Brillouin spectrum $\boldsymbol{S_e(v)}$ is the *atom* of the dictionary. We can thus define $\boldsymbol{S}$ as shifted versions of the *atom*, with the n[th] column of the matrix $\boldsymbol{S}$ being:

$$\boldsymbol{S} = \{S(v,n) = S_e(v) * \delta(v - n\Delta f_B) \mid n = 1,..,N\} \quad (12)$$

where Δf_B is the frequency shift between two adjacent sources, and N is the number of possible spectral components related to the number of segments in which the strain is assumed to be constant. Therefore, the scale of the possible local frequencies is sampled by Δf_B. Then, the algorithm estimates each weight corresponding to each component. The smaller Δf_B is, the more accurate the estimation of the spectrum will be. However, the size of the possible sources will increase, and some of them have very small amplitudes that might cause stability problems. Therefore, a sparse algorithm has to be defined to optimize the number of nonzero values into $\boldsymbol{A}$.

3) The Non-Negative Least-Square Algorithm

To solve non-negative matrix factorization, several algorithms that assure the convergence of $\boldsymbol{C}$ are available (see Lee and Seung [24], and references therein). The main drawback of these algorithms is the nonunicity of the estimated sources. This can influence the weights, and so portions of *w*, and bias the strain estimation.

As in our case the shape of the elementary Brillouin spectrum can be estimated, $\boldsymbol{S_e(v)}$, another solution is the NNLS algorithm [25]. This has been used recently in several applications, such as for blind separation in the electromagnetics field [26], and for the bioinformatics domain [27]. The problem is reformulated as follows: taking an observation column $\boldsymbol{g}$ from the Brillouin matrix $\boldsymbol{G}$, given a dictionary $\boldsymbol{S} \in \mathbb{R}_+^{\boldsymbol{N_v} \times \boldsymbol{N}}$, find the vector $\boldsymbol{a}$ minimizing:

$$\boldsymbol{c}(\boldsymbol{a}) = \frac{1}{2}\|\boldsymbol{g} - \boldsymbol{S}\boldsymbol{a}\|_2^2 \quad (13)$$

subject to the Karush-Kuhn-Tucker optimality conditions:

$$\boldsymbol{a} \geq 0 \quad (14.a)$$

$$\boldsymbol{\lambda} = \boldsymbol{\nabla c}(\boldsymbol{a}) = \boldsymbol{S}^T(\boldsymbol{S}\boldsymbol{a} - \boldsymbol{g}) \geq 0 \quad (14.b)$$

$$\boldsymbol{\lambda}^T\boldsymbol{a} = 0 \quad (14.c)$$

where $\boldsymbol{\lambda}$ corresponds to the gradient of $\boldsymbol{c(a)}$. This principle can be easily implemented by the active set algorithm presented in [28]. A passive set *Z* and an active one *R* are defined: *Z* comprises the indices of all of the amplitudes that are strictly positive of the *N* sources; *R* contains the indices of the amplitudes that are fixed at zero. First, the set *R* is filled with the *N* indices of all of the sources. An equivalent of the Lagrange multiplier, denoted as $\boldsymbol{l} = \boldsymbol{S}^T(\boldsymbol{g}\text{-}\boldsymbol{S}\boldsymbol{a})$, is calculated: the index of the maximum of $\boldsymbol{l}$ is removed from *R* and included in *Z*. Then the amplitudes are optimized to minimize $\boldsymbol{c}$. In this step, one or several amplitudes can become zero, and hence the corresponding indices go from *Z* to *R* to optimize the length of *Z*. Therefore, an optimal number of nonzero values is found. This is the main advantage of this algorithm: given *N* possibilities, it will find *P* nonzero values. Thus, for the k^{th} column of the matrix $\boldsymbol{G}$, the algorithm will find the associated weight vector $\boldsymbol{a_k}$ with P_k nonzero values among the prior *N* possibilities. As the algorithm works for one column of $\boldsymbol{G}$, this scheme is reiterated for each column, and thus we obtain the sparse matrix $\boldsymbol{A}$. It has been shown that the algorithm always converges [25]. However, there is no cut-off in the iteration required, and sometimes the computation time is very long. Another possible algorithm could be weighted least squares depending on the distortion of the spectrum.

B. Brillouin Profile Reconstruction

The goal of this section is the estimation of a Brillouin frequency profile that depends on the curvilinear abscissa. As explained above, for each acquisition point z_k on the optical fiber cable that corresponds to an integration base *w*, the algorithm provides an estimation of the amplitudes and frequencies of the components contained in the measured Brillouin spectrum. In contrast to the device algorithm, which estimates a Brillouin frequency as the abscissa of the maximum of the measured Brillouin spectrum and places it in the center of the studied portion, *w*, our decomposition algorithm finds several local frequencies. The issue is to know the layout of those frequencies within *w*.

Through our model in Eq. (8), we know that the amplitudes of the components are related to the segments (portions) of size $\widetilde{d_M}$ contained in *w* that are similarly stressed. The idea is to lay out these segments in order to estimate the Brillouin frequency profile along the optical fiber cable. The device functioning allows an overlap between two studied portions. Therefore, the common components are found between two adjacent measured spectra. We take advantage of this property to sort out the components.

First, by observing the components of three adjacent positions, $z_{k-1} = z_0 + (k-1).\Delta z$, $z_k = z_0 + k.\Delta z$ and $z_{k+1} = z_0 + (k+1).\Delta z$, it is possible to reveal a global tendency in the organization. The mean of the local Brillouin frequencies is calculated and denoted as $\bar{v}_{Bk}$. By comparing these, four simple scenarii can be defined to describe the tendencies, as shown in Table I. The example given in Fig. 4 corresponds to case 3. This means that there is a local maximum in the integration base at the k[th] position that should influence the positioning of the local frequencies. The maximum of the local frequencies in this k[th] integration base is placed in the center. The other segments, or more precisely their size $\widetilde{d_.}$, are split in two sub-ensembles. The mean of the frequency increases between z_{k-1} and z_k, and the hypothesis is to dispose the elements of the first sub-ensemble such that the related frequencies are arranged in increasing order on the left side. Mutually, the decrease between v_{Bk} and v_{Bk+1} leads to dispose the elements of the other sub-ensemble such that the related frequencies are arranged in decreasing order on the right side. Note that this method can be refined, for example, by taking into consideration the left *versus* right slope in defining the splitting operation, although such a solution is beyond the scope of the present report.

To illustrate this concept, Fig. 4a-c shows the elements (frequencies and amplitudes) of the decomposition of three distorted spectra at positions z_{k-1}, z_k and z_{k+1}. Note that the amplitudes are expressed in a relative size form (see $\widetilde{d_M}$ in Eq.

TABLE I
TENDENCIES RELATED TO THE MEANS OF THE LOCAL BRILLOUIN FREQUENCIES

Case	Frequencies comparison	Tendency
1	$\bar{v}_{Bk-1} < \bar{v}_{Bk} < \bar{v}_{Bk+1}$	Increasing
2	$\bar{v}_{Bk-1} > \bar{v}_{Bk} > \bar{v}_{Bk+1}$	Decreasing
3	$\bar{v}_{Bk} > \bar{v}_{Bk-1} > \bar{v}_{Bk+1}$ $\bar{v}_{Bk} > \bar{v}_{Bk+1} > \bar{v}_{Bk-1}$	Local maximum
4	$\bar{v}_{Bk-1} > \bar{v}_{Bk+1} > \bar{v}_{Bk}$ $\bar{v}_{Bk+1} > \bar{v}_{Bk-1} > \bar{v}_{Bk}$	Local minimum

(8)); i.e., the sum of the segments represented for example in Fig. 4a is equal to the size of the integration base, *w*. We assume here that position z_{k-1} was previously identified as a first-case scenario. This means that the segments that correspond to position z_{k-1} should be arranged such that the related frequencies are in increasing order (see Fig. 4d). We also assume that the position z_{k+1} will be identified in the next step as the second-case scenario. This means that the segments that correspond to position z_{k+1} will be arranged such that the related frequencies are in decreasing order (see also Fig. 4d). For the elements related to the z_k position, these are arranged in Fig. 4d as previously explained: the maximum of the local frequencies in the center, increasing on the left side and decreasing on the right side.

Secondly, as there is spatial redundancy, the superposition of several frequencies can appear over several portions, as can be seen in Fig. 4d. We propose here to compute the mean of the superposed frequencies while using a nonoverlapping sliding window of length Δx:

$$v_B(x) = \frac{1}{Q}.\sum_{\substack{j=1 \\ x\in\Delta x}}^{Q} v_{Bj}(x), \qquad (15)$$

where Q is the number of estimated local frequencies v_B that exist within Δx. Finally, we estimate a Brillouin frequency profile that depends on the distance $\boldsymbol{x}$, with a new spatial resolution of Δx. Fig. 4e shows the Brillouin frequency obtained for the rearranged estimated local frequencies of Fig. 4d. The user has to choose the size Δx of the sliding window, which is another parameter that will be discussed later.

The next section is dedicated to applications to numerical and experimental datasets, and this shows that the proposed method can enhance the Brillouin frequency distribution estimation along the distance.

IV. RESULTS AND DISCUSSION

We first applied the proposed methodology to estimate the Brillouin frequency profile with a new spatial resolution on a numerical dataset built through the model in Eq. (6). Discussion about the influence of the parameters is provided. Then, the proposed methodology is tested on an experimental dataset acquired under controlled conditions.

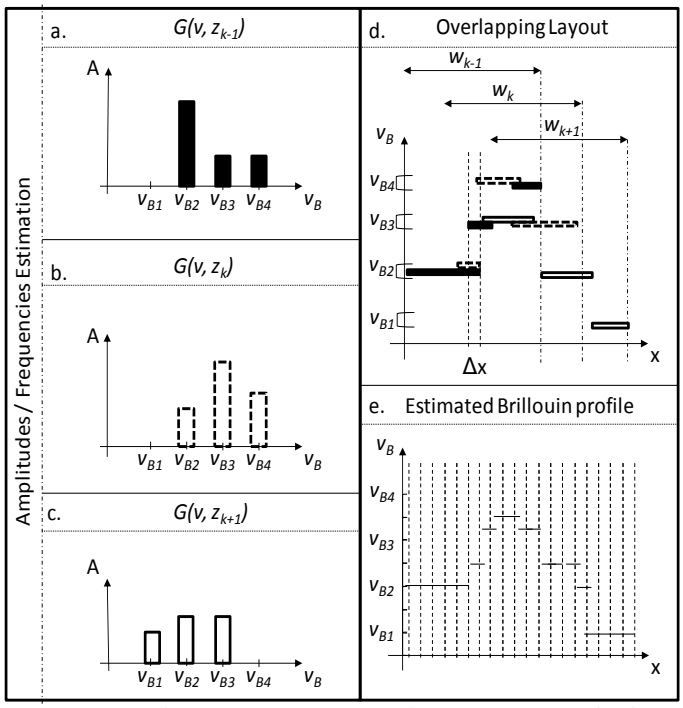

Fig. 4. Example of the layout methodology to find the Brillouin profile for the third-case scenario. (a-c) Elements (amplitudes and frequencies) of the NNLS decomposition of three distorted spectra at positions k-1, k, and k+1. (d) Overlapping layout. (e) Estimation of the Brillouin profile that depends on distance, with new spatial resolution Δx.

A. Numerical Dataset

1) Description

First, a numerical dataset is built using a Brillouin frequency profile as input. The profile shown in Fig. 5a was chosen to present several kinds of local frequency variations to test the algorithm in different configurations. Five areas can be identified and are shown in Fig. 5a: a null slope over the first 2 m, and from 8 m to 10 m, denoted as '0'; a positive slope between 2 m and 4.6 m, and from 7.5 m to 8 m, denoted as '+'; a local maximum at a frequency of 10.92 GHz and a distance of 4.6 m, denoted as 'max'; a decreasing slope between 4.6 m and 6 m to 10.72 GHz, denoted as '-'; and local variations between 6 m and 7.5 m, denoted as 'min', and comprising one local maximum and two local minima.

To build a data matrix **G**, as in Eq (9), the parameters were chosen as follows: a frequency sampling of Δv = 1 MHz for a total acquisition frequency N_v = 600 covering the 10.5 GHz to 11.1 GHz band; an integration base w = 1 m; a spatial resolution Δz = 40 cm; and a number of acquisition points N_L = 40 that simulate a 10-m optical fiber cable. A classical pseudo-Voigt distribution was used to simulate the elementary Brillouin spectrum ***Se(v)***. These parameters are classically encountered for industrial B-OTDA units. The constructed data matrix **G** is shown in Fig. 5b. As expected by the theory of Brillouin distortion phenomenon, when the slopes of the curve are important within *w*, the resulting Brillouin spectrum is distorted. This is mostly visible between 2 m and 4.6 m, 4.6 m and 6 m, and 7.5 m and 8 m.

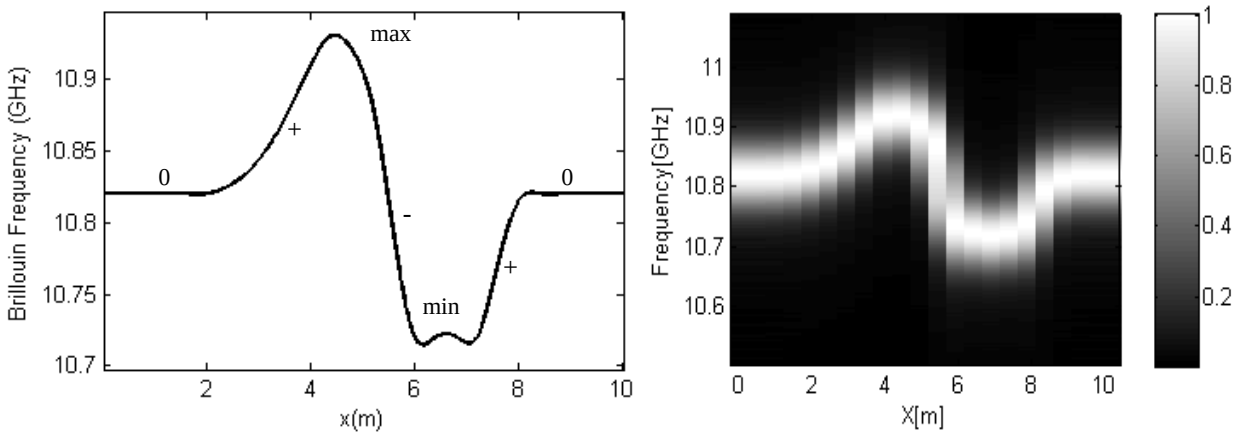

(a) (b)

Fig. 5. (a) Numerical Brillouin frequency profile that depends on the curvilinear abscissa *x*, in GHz. (b) The associated normalized Brillouin spectrum matrix with acquisition parameters of w = 1 m and Δz = 40 cm. The color scale is related to a normalized gain.

2) Results and Discussion

The proposed algorithm is applied to the Brillouin spectrum matrix. The source dictionary $\boldsymbol{S}$ is constructed with the same elementary Brillouin spectrum ***Se(v)*** used to construct the Brillouin spectrum matrix $\boldsymbol{G}$. The dictionary constructed with $\Delta f_B = 1MHz$ is shown in Fig. 6a. As the frequencies span between 10.5 GHz and 11.1 GHz, the size of $\boldsymbol{S}$ is $N_v = 600 \times N = 600$. With this dictionary, the NNLS algorithm is applied to the numerical Brillouin, and the estimated P nonzero values among the N possibilities as explained in section III.1. These are shown in Fig. 6b according to the distance and the local Brillouin frequency. As observed, from 0 m to 1.4 m and from 8.6 m to 10 m, where the Brillouin spectrum is not distorted, $P = 1$. It is obvious that P increases with the importance of the spectrum distortion. This correlates with the increase in the number of spectral components contained in the distorted spectrum. For z = 4.6 m, P has the highest value and corresponds to the most distorted spectrum. A new spatial sampling is chosen at Δx = 5 cm. The estimated Brillouin profile can be compared to the reference profile, as shown in Fig. 6c. The qualitative approach enables the validation of the methodology: except where the slope of the curve is very high, the estimated profile is mixed in with the reference profile.

a) Choice of the Brillouin Frequency Sampling Δf_B

The frequency shift Δf_B is a major parameter in the proposed method: it defines the sampling of the local Brillouin frequency. Therefore, if Δf_B increases, then the number of possible spectral components N will decrease, although the Brillouin frequency sampling will not be precise enough. In this case, according to Eq. (7), the reconstructed spectrum will not correctly fit the spectrum measured.

To study the influence of the frequency sampling Δf_B on the estimated Brillouin profile, we chose several values between 1 MHz and 10 MHz. For this study, we fixed the new spatial sampling to Δx = 1 cm. For each Δf_B, we apply the step described above and estimate a Brillouin profile. For quantitative analysis, we can calculate the relative mean square error (RMSE) between the reference Brillouin profile and the estimated profile. The RMSE for the five areas highlighted in Fig. 6c with respect to the different values of Δf_B are shown in Fig. 6d, which highlights that the quantification errors of the profile are highly dependent on the value of Δf_B. Globally, with increasing Δf_B, the RMSE increases whatever the kind of slope. For the smallest quantification error, it is important to fix a small Δf_B. On the other hand, if Δf_B is too small, the calculation time increases significantly, as well as the size of the dictionary.

b) Choice of the new spatial sampling Δx

Applying the Brillouin profile reconstruction algorithm, a Brillouin frequency profile is estimated. As previously explained, we first rearrange the segments within each integration base of size w located at position z_k based on a tendency, then we apply an averaging step with a new spatial resolution Δx. This second step can remove some misplacement defects, although it also misses some local frequency variations. Therefore, an optimal value of Δx has to be found to ally the small spatial resolution with a precise reconstruction. To study the influence of this parameter, we chose several values from 40 cm to 1 cm, with Δf_B fixed to 1 MHz, the value that gave the smallest RMSE. Then, we computed the RMSE between the estimated profile and the reference profile; i.e., the Brillouin profile used to construct the Brillouin spectrum matrix. The RMSE for the five areas highlighted in Fig. 6c with respect to the different values of Δx are shown in Fig. 6e, which shows that the averaging step can miss local variations. Depending on Δx, the errors are relatively constant when the slope is null, and then they decrease where there are local minima and maxima. Where there are positive slopes, the errors increase. As the slope is less important between 2.5 m and 4 m, the error is smaller than between 7.8 m and 8 m. The higher RMSE is where there is the greater gradient. Our algorithm is then sensitive to the slope: the greater the gradient, the higher the errors. Small numbers of cases have been picked and may misplace some sub-resolution elements and hence will not deliver the resolution as expected. This limitation is revealed big changes that happen into a short

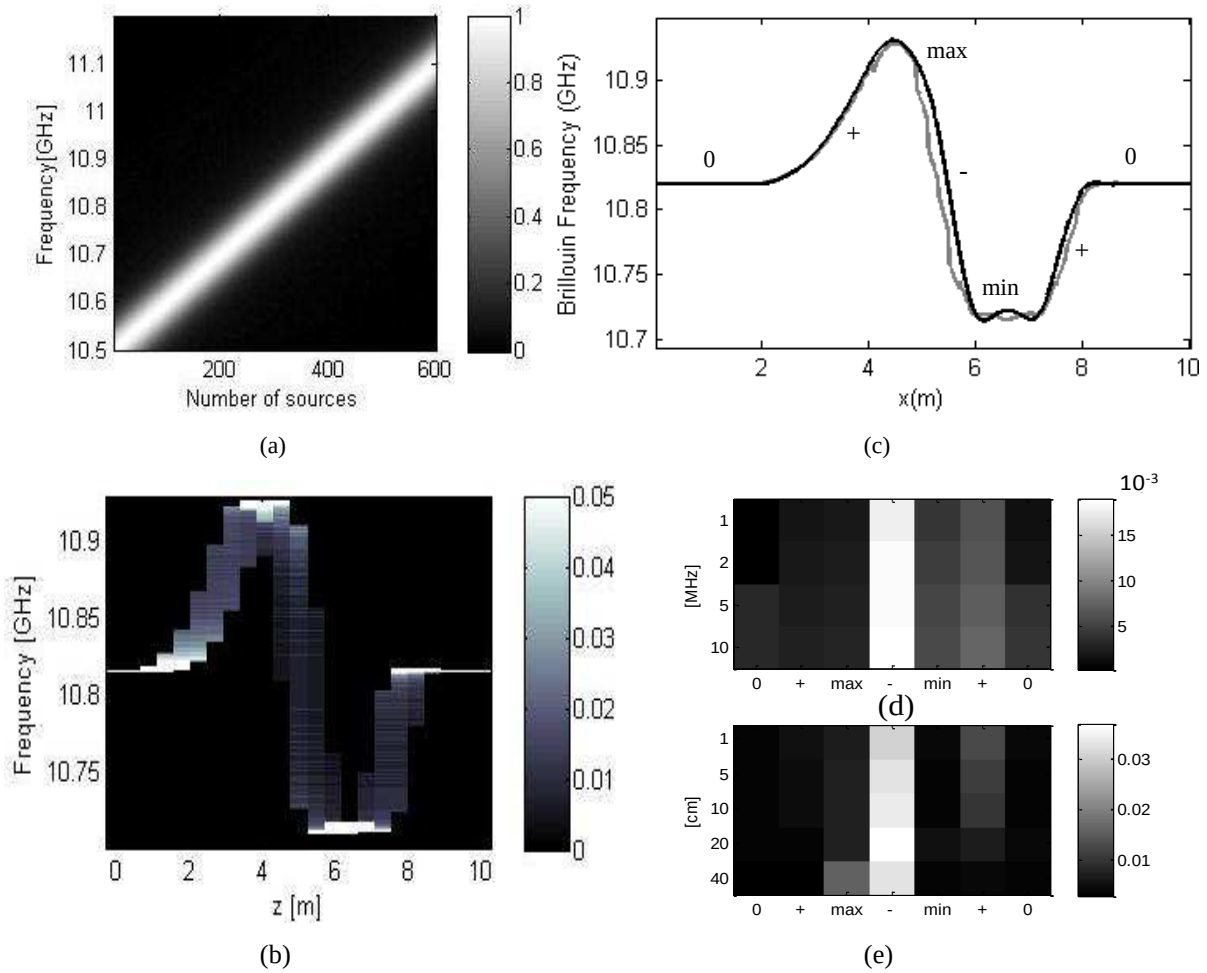

Fig. 6. (a) Dictionary of sources with frequency shift Δf_B of 1 MHz between 10.5 GHz and 11.15 GHz. (b) The amplitudes found for the sources contained in the dictionary for each integration base, located at positions z_k. The scale corresponds to a normalized gain with a threshold at 0.05% of the maximum. (c) Superposition of two Brillouin profiles: the input (black line) used to construct the Brillouin spectrum matrix; the estimation using the proposed algorithm (gray line) with Δx = 1 cm. (d) Relative errors between the estimated Brillouin profile and the reference profile for several values of Δf_B and a fixed spatial resolution of Δx = 1 cm. (e) Relative errors between the estimated Brillouin profile and the reference profile for several values of the spatial resolution and for a frequency shift Δf_B of 1 MHz.

distance at the expense of losing accuracy for small variations. As seen in Fig. 6(c), the local maximum is not retrieved in the reconstruction. The follow-up of our study will be for the improvement of this algorithm. Nevertheless, in response to several local trials, the proposed algorithm can be used to find a profile that integrates local and global variations with much smaller spatial resolution; i.e., 5 cm instead of 40 cm. As the first result is encouraging, the methodology was tested on an experimental dataset.

B. Experimental Dataset

1) Description

A trial was carried out in an EDF laboratory under controlled conditions. An industrial optical fiber cable composed of several optical fibers wrapped in a protective coating was used with two industrial devices: a Rayleigh OBR and a B-OTDA. The OBR was a Luna Technologies device, with the following characteristics: 1-cm spatial resolution over 70 m, with a precision of 1 µm/m and 0.1 °C [20]. The industrial B-OTDA unit, known as a DITEST STA-R, and furnished by Omnisens, can measure strain and temperature over 20 km with a precision of 20 µm/m and 1 °C. The acquisition parameters were: integration base w = 1 m, spatial resolution Δz = 40 cm, and frequency sampling Δv = 1 MHz. The cable was installed between two fixed points, denoted x_1 = 10.5 m and x_2 = 14 m. During the experiment, the temperature was controlled and its variation can be considered as negligible. Therefore, the frequency variations were only linked to the strain changes, with reference to Eq. (10).

A first acquisition was performed using both of the devices when the cable was relaxed: the initial state A. Then, the cable was pulled between the fixed points, which induced a stressed state, state B, with another acquisition performed with both of the devices. The B-OTDA raw data are shown in Fig. 7a, b for the two states of the optical fiber cable. From these matrices, the device provides Brillouin frequency profiles that are estimated as the abscissa of the maximum of each measured Brillouin spectrum, as the profiles that are plotted in crossed lines in Fig. 7a, b. As can be seen, the Brillouin frequency increased in the stressed area between x_1 and x_2.

The B-OTDA strain profile output with a spatial resolution of Δz = 40 cm is plotted in Fig. 7c (circles), whereas the OBR strain profile output with a spatial resolution of 1-cm is plotted as the dotted line in Fig. 7c. As the OBR has a centimeter spatial resolution, it will be considered in the present study as the reference strain profile for the two states of the fiber. In

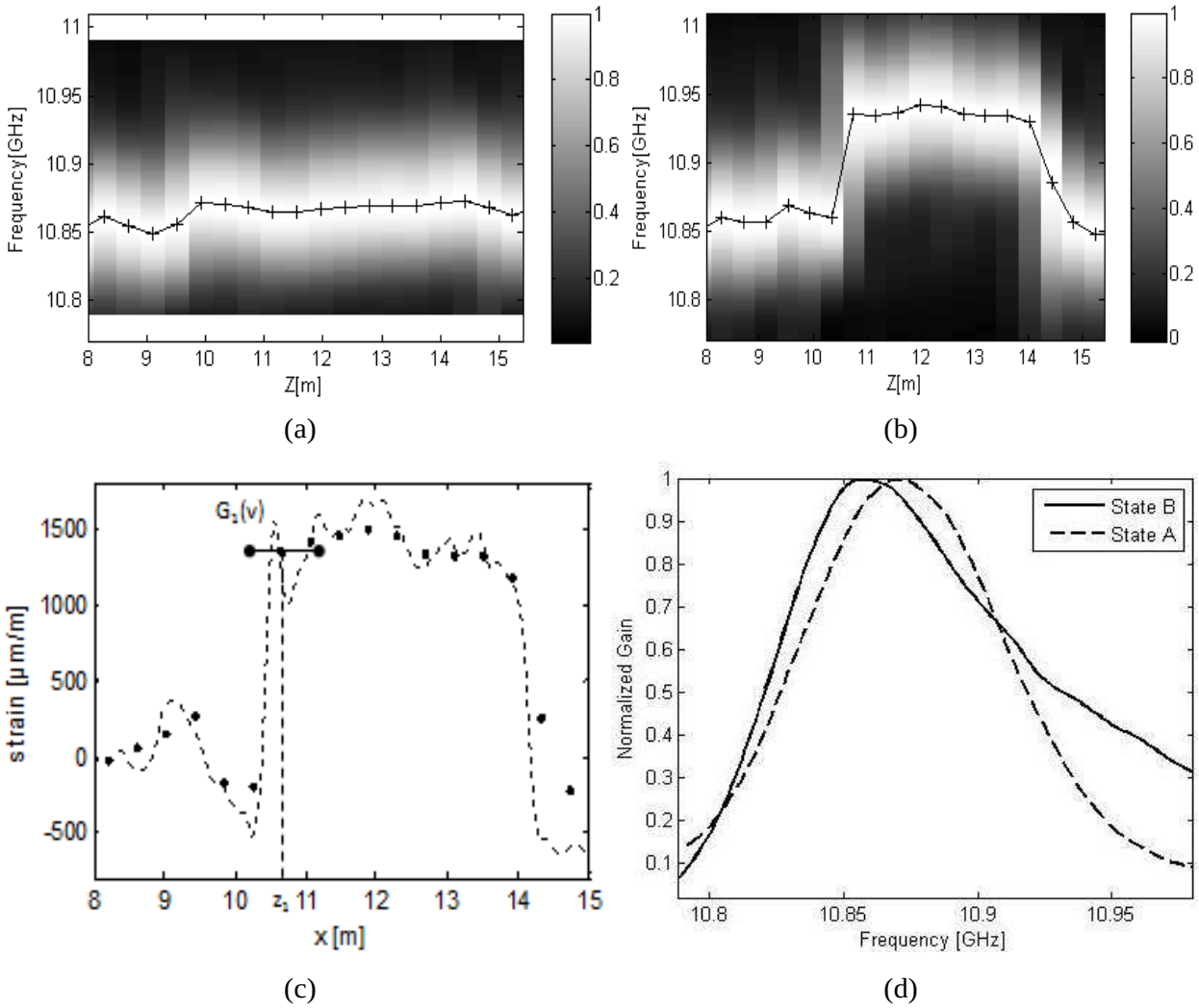

Fig. 7. (a, b) Normalized Brillouin spectrum matrices and the B-OTDA Brillouin frequency profile (crossed line) for the two states of the optical fiber: state A (initial state; a); state B, (stressed state; b). The acquisition parameters were w = 1 m, Δz = 40 cm, $\Delta \nu$ = 1 MHz. c. Strain profile provided by the OBR (Rayleigh) with centimeter spatial resolution (dotted line) and the Brillouin device (circles). d. Normalized Brillouin spectra $G(\nu,z_k)$ at a fixed distance z_k = 10.6 m for state A (dotted line) and state B (continuous line).

this strain measurement, several areas can be distinguished: from 8 m to 10.2 m, the profile varies between -500 µm/m and 500 µm/m over a few meters; and a high strain variation from -500 µm/m to 1500 µm/m appears afterwards, within a few centimeters; from 10.5 m to 14 m, the profile varies between 1000 µm/m and 1550 µm/m with a peak with a width of 15 cm; there is another high strain variation at around 14 m, where the strain evolves from 1200 µm/m to -600 µm/m within a few centimeters; finally, the strain is relatively constant from 14 m to 15.3 m.

In comparison with the OBR output, the B-OTDA profile follows the global strain and misses some high-strain variations, such as for z = 10.6 m and after z = 14 m. At z_1 = 10.6 m, the integration base w is shown in Fig. 7c by a continuous line segment. As can be seen, within w, the strain variations are high within a few centimeters. As explained in Section II, the measured Brillouin spectrum will be distorted at the position z_1 = 10.6 m. The measured Brillouin spectrum $\boldsymbol{G(\nu,z_1)}$ is plotted in Fig. 7d for the two states of the optical fiber. Indeed, from a symmetric distribution, this evolves into an asymmetric and broadening spectrum.

Therefore, the algorithm of the industrial device is not sufficient to detect important and local events in the structure, such as cracks. The proposed algorithm will be applied on the two Brillouin spectrum matrices recorded by the B-OTDA device, to estimate a new strain profile. Our goal is to estimate this strain profile with optimal spatial resolution and the best strain precision.

2) Results and Discussion

First of all, the elementary Brillouin spectrum $\boldsymbol{S_e(\nu)}$ has to be estimated in order to apply our methodology. Taking into account Eq. (5), the elementary Brillouin spectrum can be found when no strain is imposed within the integration base. Under our experimental conditions, several meters of cable were laid with no stress. The Brillouin spectra were acquired for these positions, denoted here as z_{01}, z_{02}, …, z_{0M}. At each position, the measured Brillouin spectrum $\tilde{G}(\nu, z_{0M})$ will approximate $\boldsymbol{S_e(\nu)}$. The elementary Brillouin spectrum $\boldsymbol{S_e(\nu)}$ is estimated as the mean of these spectra; i.e.:

$$\boldsymbol{S_e(\nu)} = \frac{1}{M}\sum_{p=1}^{M} \tilde{G}(\nu, z_{0p}) \qquad (16)$$

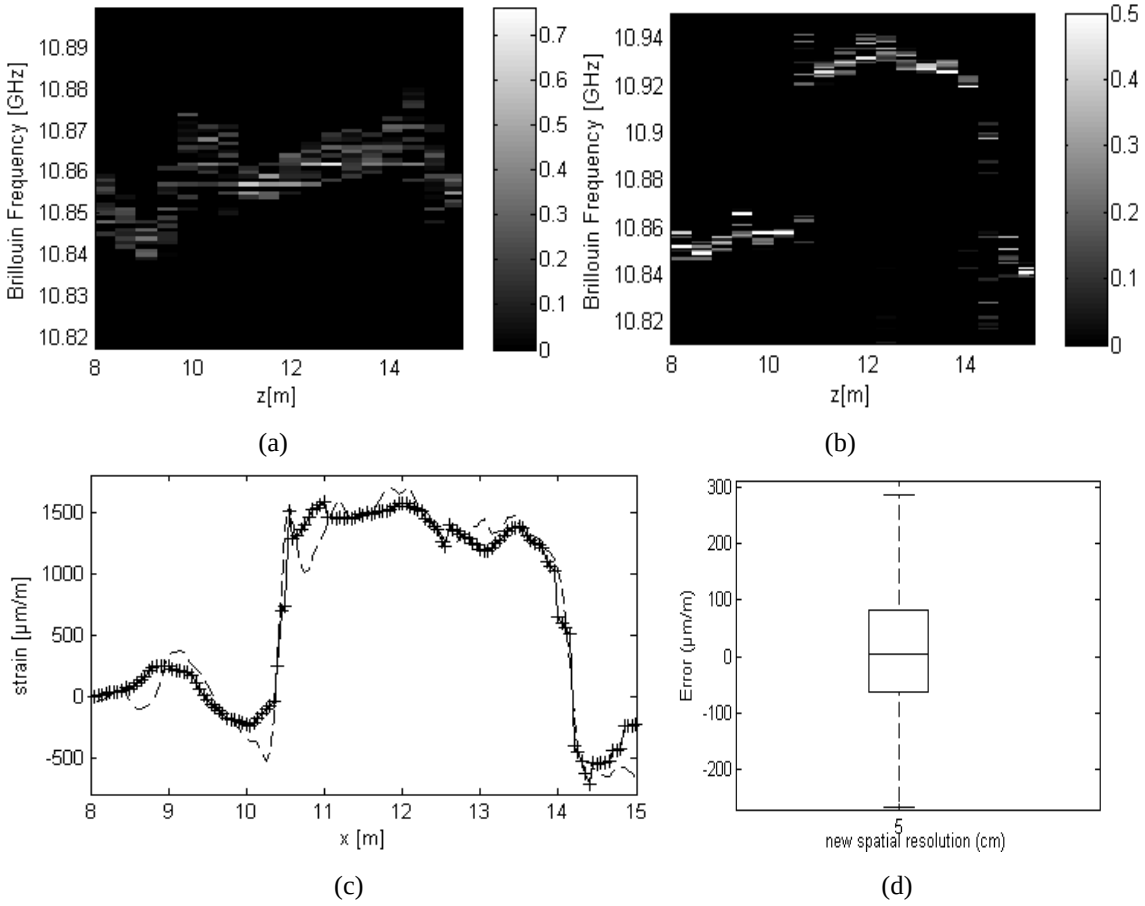

Fig. 8. (a, b) Decomposition of the Brillouin spectra acquired in the defined source dictionary for the initial state A (a) and the stressed state B (b). The scales correspond to the normalized gain. (c) Several strain profiles: the output from the OBR (dotted line) and the estimation by the proposed methodology (crossed line). (d) Box plot representation of the errors between the reference strain profile (OBR) and the estimated profile.

The source dictionary $\boldsymbol{S}$ is then constructed using Eq. (12) with Δf_B = 1 MHz. As the frequency span varies between the two states, the number of possible spectral components *N* will differ, although Δf_B has to be the same to have the same quantification error for both of the estimated Brillouin profiles.

The NNLS algorithm is applied to both of the Brillouin spectrum matrices. This decomposition enables local Brillouin frequencies, with their associated amplitudes, to be found. The estimated amplitude matrices are shown in Fig. 8a, b, where the kth column of each image represents the relative amplitudes $\widetilde{d_M}$ (see Eq. (8)) for position z_k. As observed in the first matrix, few components are found in the spectra. The Brillouin frequency distribution is centered around 10.86 GHz, with a small standard deviation. This means that the strain is relatively constant within *w*. In the second matrix, the standard deviation is much more important, especially for several positions of z_k where the spectrum is distorted; e.g., at z_k = 10.6 m. In such cases, the number *P* of the estimated spectral components increases, because the spectrum is much more distorted, as can be seen in Fig. 7d.

The Brillouin profile reconstruction step was applied to the estimated amplitude matrices with new spatial resolution Δx = 5 cm. This choice was made with respect to the results obtained with the numerical data discussed above. Two Brillouin frequency profiles were estimated, one for state A (initial state) and one for state B (stressed state). These profiles are not shown here. Then, through Eq. (10), a strain profile was estimated, which is shown in Fig. 8c. As can be seen, compared with the OBR reference strain profile, our methodology can detect and localize very high strain variations within *w*, such as for the peak located between 10.5 m and 11 m.

For a quantitative comparison, the error between the reference profile and the estimated profile is shown as a Tukey box plot in Fig. 8d. The median is equal to 4.6 µm/m, the error is essentially contained between -265 µm/m and 286 µm/m, and 50% of the errors are between -61 µm/m and 81 µm/m. This is satisfactory, as the strain variations are of the order of 1000 µm/m.

This result validates the source separation methodology for the improvement of the accuracy and spatial resolution of the industrialized device. Our proposed method enables the sensor model to be simplified, as the signal processing approach needs fewer steps than the state-of-the-art approach, such as that presented in [17]. In terms of computational costs, our decomposition and reconstruction steps are short time consuming (few seconds) whereas for a similar configuration, the state-of-art approach needs less than 5 min with a standard desktop computer.

V. Conclusion

In this report, we have addressed the problems of the improvement of the accuracy and spatial resolution of

industrial B-OTDA devices. A method to estimate the strain profile in an optical fiber cable using the Brillouin spectrum matrix measured by a B-OTDA unit is proposed. We first described a signal processing approach to model the device behavior. The state-of-the-art models are based on optical physics and fitted experimental devices. Our model is based only on the elementary Brillouin spectrum that can be estimated for portions of cable laid out with no stress. We have shown how it is possible to model Brillouin spectrum distortion: if the strain is not constant, the elementary Brillouin spectrum is frequency-shifted locally and integrated within the base integration. Therefore, the spectrum measured by a B-OTDA device can be seen as a sum of the elementary Brillouin spectra centered on the local Brillouin frequencies. Using this model, and with the help of techniques based on data decomposition and source separation, we can identify the amplitudes and frequencies of the spectral components contained in the measured distorted Brillouin spectrum. The amplitudes of the components are associated with portions within the integration base. We proposed a methodology based on the spectral component characteristics to estimate the Brillouin frequency profile with new spatial resolution.

Numerical data enabled the quantification of the error between a simulated Brillouin frequency profile and the estimated profile, which allowed the identification of the optimal parameters. Optimal spatial resolution was found as 1 cm, which is a significant improvement when compared with the 40-cm spatial resolution of industrial B-OTDAs. This resolution provides the best ratio between the smallest spatial resolution and the higher precision of the reconstruction.

To fully validate the methodology, an experiment was carried out under controlled conditions. A complementary OBR that provided strain profile measurements with centimeter spatial resolution was used as the reference. This device cannot be used in long-range applications, as the sensor length is limited to 70 m. The Brillouin frequency matrices were acquired by the industrial device for the two states of the optical fiber cable. Our algorithm allowed the estimation from these matrices of a strain profile with a new spatial resolution of 5 cm. This estimation was compared with the strain profile output of the reference OBR (at 1-cm spatial resolution) and with the internal algorithm of an industrial B-OTDA device (at 40-cm spatial resolution). Unlike the device algorithm, the proposed algorithm allows the detection and localization of high strain variations. Some improvements can be made to the profile reconstruction algorithm to enhance the accuracy. On the other hand, other source separation algorithms or sparsity criteria can be tested. As the modeling of the recorded Brillouin spectra by the device is validated, an inverse method can also fit such a problem. The development of this methodology for Brillouin spectrum matrices acquired on large structures will form the follow-up to this study.

REFERENCES

[1] B. Vogel, C. Cassens, A. Graupner, and A. Trostel, “Leakage detection systems by using distributed fiber optical temperature measurements,” in *Proc. SPIE Smart Structures and Materials*, CA, USA, vol. 4328, pp. 23–34, 2001.

[2] S. Johansson and P. Sjodahl, “Downstream seepage detection using temperature measurements and visual inspection monitoring experiences from Røsvatn field test dam and large embankment dams in Sweden,” in *Proc. Intl. Seminar on Stability and Breaching of Embankment Dams*, Oslo, Norway, p. 21, 2004.

[3] A. Rozycki, J. M. Ruiz, and A. Caudra, “Detection and evaluation of horizontal fractures in earth dams using the self potential method” in *Engineering Geology*, vol. 82, no. 3, pp. 145–153, Jan. 2005.

[4] P. Sjodahl, T. Dahlinb, S. Johansson, and M. H. Lokec, “Resistivity monitoring for leakage and internal erosion detection at hllby embankment dam,” in *Journal of Applied Geophysics*, vol. 65, pp. 155–164, 2008.

[5] V. Lanticq, R. Gabet, F. Taillade, and S. Delepine-Lesoille, “Distributed optical fibre sensors for structural health monitoring: upcoming challenges”, in *Optical Fiber, New Developments*, Chapter 9, 2009.

[6] J.M. Hénault, M. Quiertant, S. Delepine-Lesoille, J. Salin, G. Moreau, F. Taillade, and K. Benzarti, “Quantitative strain measurement and crack detection in RC structures using a truly distributed fiber optic sensing system”, in *Construction and Building Materials*, vol. 37, pp. 916–923, 2012.

[7] M. Nikles, R. Burke, F. Briffod, and G. Lyons, “Greatly extended distance pipeline monitoring using fiber optics”, in *Proc. of OMAE05*, Halkidiki, Greece, , June 2005.

[8] M. Nikles, “Long-distance fiber optic sensing solutions for pipeline leakage, intrusion and ground movement detection”, in *Proc. of the 6th Fiber Optic Sensors and Applications (SPIE ‘09),* pp. 731602-731613, April, 2009.

[9] J.M. Lopez-Higuera, L. Rodriguez Cobo, A. Quintela Incera, and A. Cobo, "Fiber optic sensors in structural health monitoring," in *Journal of Lightwave Technology*, vol. 29, no. 4, pp.587–608, 2011.

[10] S. Yin and F. T. S. Yu, “Distributed fiber optic sensors”, in *Optical Engineering*, Ed. New-York Marcel, 2002.

[11] A. A. Khan, V. Vrabie, J. I. Mars, A. Girard, and G. D’Urso, “A source separation technique for processing of thermometric data from fiber-optic DTS measurements for water leakage identification in dikes” in *IEEE Sensors Journal*, vol. 8, no. 7, pp. 1118–1129, 2008.

[12] S. Blairon, J-M. Hénault, E. Buchoud, G. Vinceslas, and S. Delepine-Lesoille, “Truly distributed optical fiber extensometers for geotechnical structure monitoring (dikes and underground repository): Influence of sensor external coating” in *8th Int. Symp. of FMGM*, Berlin, Germany, September 2011.

[13] M. Frogatt and J. Moore, “High-spatial-resolution distributed strain measurement in optical fiber with Rayleigh scatter” in *Applied Optics*, vol. 37, no. 10, pp. 1735-1740, 1995.

[14] X. Bao, J. Dhliwayo, N. Heron, D. J. Webb, and D. A. Jackson, “Experimental and theorical studies on a distributed temperature sensor based on Brillouin scattering,” in *Journal of Lightwave Technology*, vol. 13, no.7, pp. 1340–1348, 1995.

[15] X. Bao and L. Chen, “Recent progress in Brillouin scattering based on fiber sensors,” in *Sensors*, vol.11, pp. 4152–4187, 2011.

[16] F. Ravet, X. Bao, T. Ozbakkaloglu, and M. Saatcioglu, “Signature of structure failure using asymmetric and broadening factors of Brillouin spectrum”, in *IEEE Photonics Technology Letters*, vol. 18, no. 2, pp. 394–396, 2006.

[17] F. Ravet, X. Bao, Y. Li, Q. Yu, A. Yale, V. P. Kalosha, and L.Chen, “Signal processing technique for distributed Brillouin sensing at centimeter spatial resolution*”,*in *Journal of Lightwave Technology*, vol. 25, no. 11, pp. 3610–3618, 2007.

[18] E. Buchoud, S. Blairon, G. D’Urso, J-M. Henault, A. Girard, J. Mars, and V. Vrabie, “Detection of ground movement using the shape of Brillouin spectrum”, presented at the *Near Surface Geoscience*, Paris, France, September 2012.

[19] J. Smith, A. Brown, M. demarchant, and X. Bao, “Pulse width dependence of the Brillouin loss spectrum*”* in *Optics Communication* vol.168, no.5-6, pp. 393–398, 1999.

[20] B. Soller, D. Gifford, M. Wolfe, and M. Froggatt, “High resolution optical frequency domain reflectometry for characterization of components and assemblies”, in *Optics Express*, vol. 13, pp. 666-674, 2005.

[21] A. Sang, M. Froggatt, D. Gifford, S. Kreger, and B. Dickerson, “One-centimeter spatial resolution temperature measurements in a nuclear reactor using Rayleigh scatter in optical fiber”, in *IEEE Sensors Journal*, vol. 8, pp. 1375–1380, 2010.

[22] T. Horiguchi and M. Tateda, “B-OTDA-nondestructive measurement of single-mode optical fiber attenuation characteristics using Brillouin interaction: theory,” in *Journal of Lightwave Technology,* vol. 7, pp. 1170–1176, 1989.

[23] X. Bao, A. Brown, M. DeMerchant, and J. Smith, "Characterization of the Brillouin-loss spectrum of single-mode fibers by use of very short (<10 ns) pulses", in *Optics Letters*, vol. 23, no. 8, pp. 510-512, 1999.

[24] D. D. Lee and H. S. Seung, "Algorithm for non-negative matrix factorization", in *Advances in neural information processing systems*, vol. 13, pp. 556–562, 2001.

[25] C. L. Lawson, and R. J. Hanson, "Linear least squares with linear inequality constraints" in *Solving Least Squares Problems*, Ed. Prentice-Hall, Englewood Cliff NJ, 1974.

[26] M-H. Wei, W. R. Scott, and J. H. McClellan, "Robust estimation of the discrete spectrum of relaxations for electromagnetic induction responses", in *IEEE Trans. on Geosciences and Remote Sensing*, vol. 8, pp. 1169–1179, 2009.

[27] D. Repsilber, S. Kern, A. Telaar, G. Walzl, G. F. Black, J. Selbig, S. K. Pardia, S. HE. Kaufmann, and M. Jacobsen, "Biomarker discovery in heterogeneous tissue samples-taking the *in-silico* confounding approach", in *BMC Bioinformatics*, vol.11, pp. 27–42, 2010.

[28] R. Bro and S. De Jong, "A fast non-negativity-constrained least squares algorithm", in *Journal of Chemometrics*, vol. 11, pp. 393–401, 1997.